Fachtagung "Experimentelle Strömungsmechanik"
5. – 7. September 2017, Karlsruhe

Untersuchung junger Blattspitzenwirbel an einem Rotorteststand mittels stereoskopischer PIV

Investigation of young blade-tip vortices at a rotor test facility using stereoscopic PIV

Johannes N Braukmann, Till Schwermer, C Christian Wolf
Deutsches Zentrum für Luft- und Raumfahrt e.V., Bunsenstraße 10, 37073 Göttingen,
johannes.braukmann@dlr.de

Wirbel, Rotor, PIV
vortex, rotor, PIV

Abstract

To investigate the blade-tip vortices on a new rotor test stand at the German Aerospace Center (DLR) in Göttingen stereoscopic PIV measurements were carried out. The test cases were performed with a cyclic variation of the blade pitching angle which leads to a dynamic flow separation ("dynamic stall") over approximately 40% of the period. The vortex roll-up and development were recorded over one period at five radial planes between $7°$ and $40°$ behind the $c/4$-line of a rotor blade. After an automated detection of the vortex center positions, characterizing parameters such as the tangential velocity, the circulation and the vortex core size were calculated. The dataset allows for a detailed description of the vortex strengths and their size. Furthermore, radial distributions of relevant vortex parameters were derived, which allows for a more detailed characterization of the vortex topology. During dynamic stall a strong influence of the blades wake on the vortex development was found.

Introduction

Helicopter rotor blades produce tip vortices due to the generation of lift. This general behavior is comparable to fixed-wing aircrafts although the topology of rotor aerodynamics is characterized by highly unsteady flow. In contrast to the wing-tip vortices on fixed-wing aircrafts, the blade-tip vortices can interact with subsequent blades under certain conditions. These blade-vortex interactions (see Poling et al. 1989) are one of the main sources of sound and vibration emissions on a helicopter. Therefore a detailed understanding of the generation, the propagation and also the decay of the tip vortices is desirable and has been subject to research for many years (see e.g. Tangler 1977). Within the last years the German Aerospace Center (DLR) in Göttingen conducted several investigations concerning blade-tip vortices either on a pitching blade-tip (see Wolf et al. 2016) or on a Mach-scaled rotor (see Bauknecht et al. 2017).
For further research projects a rotor test facility (RTG) was set up by Schwermer et al. 2016. The measurements described within the current paper aim to investigate the blade-tip topology of this new test stand. For this purpose stereoscopic particle image velocimetry (PIV) was used.

Theoretical Background

When generating lift, a pressure difference between upper and lower side of a profile occurs. In case of a finite wing this difference leads to a flow around the wing tip. This flow phenomenon then forms the blade tip vortex. Within the roll-up of a vortex, the wake flow of the rotor blade is entrained into the rotational fluid motion. This effect influences the vortex development over its age and can change the vortex properties to either a rising strength or to a faster dissipation of the vortex.

The rotational movement of a vortex leads to a tangential velocity (V_{tang}) with respect to the vortex center. To quantify the strength of a vortex the circulation Γ is most commonly used. Γ is defined as the integral of the vorticity (which describes the rotational motion of the fluid) within a defined region or the ring integral of the tangential velocity V_{tang}. For rotationally symmetric vortices this integral simplifies to the product $\Gamma = 2\,\pi\,r\,V_{\text{tang}}(r)$. According to the theorems by Helmholtz and Kutta-Zhukovsky the overall circulation of a blade-tip vortex $\Gamma(r \to \infty) = \Gamma_0$ can be linked to the generated lift of the blade.

On helicopter rotors a helical vortex structure forms due to the rotational movement of the rotor blades. Therefore subsequent blades may interact with the vortices of preceding blades under certain flight conditions. To investigate and understand the blade-vortex interaction a more detailed analysis of vortices is needed. To further characterize the spatial structure of a vortex, additional parameters such as radial distributions of e.g. V_{tang} and Γ can be analyzed. The radial position of the highest tangential velocity $V_{\text{tang, max}}$ is defined as the vortex core radius r_{c}, which provides a measure of the compactness of the vortex.

In case of the current measurement the pitch angle of the blades was varied as a function of the azimuth angle using a swashplate. This cyclic pitch input simulates the blade control of a helicopter rotor in forward flight. It has an additional influence on the vortex generation and development, since the vortex formation then depends on the azimuthal position and the local angle of attack. For example the rapid change from attached flow to separated flow and then back to attached conditions within dynamic stall can cause strong gradients within a vortex over the azimuth.

Using PIV all information needed for a comprehensive vortex analysis can be measured. A drawback of this technique is the so called “particle void” in the vortex center. Centrifugal forces in the vortex push the denser PIV seeding particles out of the center region. This effect defines the minimal radius at which PIV yields usable data. In the past it was common to identify the particle void as vortex core (see Young 2003). However, this direct connection is only a very rough approximation. The current investigation will show that the maximum tangential velocity is often located outside of the void, which simplifies the interpretation of the PIV results.

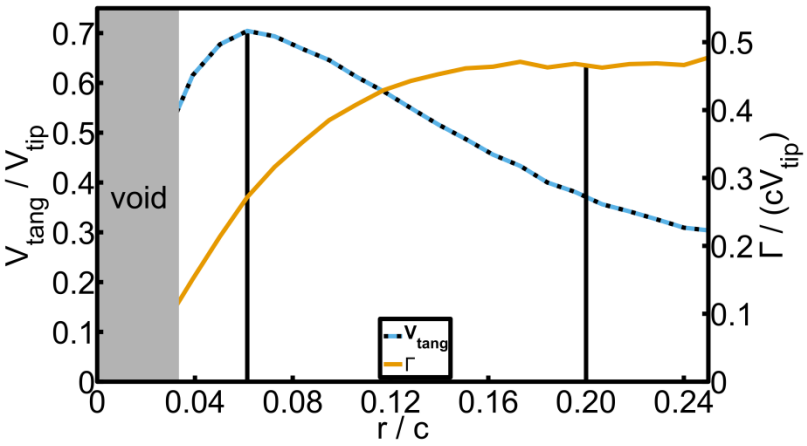

Figure 1: Radial distribution of tangential velocity and circulation for $t/T = 0.4$ and $\Psi_{\text{V}} = 10°$.

In Fig. 1 an example of a

tangential velocity profile as well as of a circulation distribution are presented. Furthermore the core radius at the position of highest tangential velocity V_{tang} and the location of $r = 0.2c$ are marked. As described before, the lack of particles in the vortex center leads to an area of unreliable data and has thus to be ignored in the analysis.
Because of this lack of information around the vortex center, a void larger than the core radius leads to an underestimation of the maximal tangential velocity and also to an overestimation of the core radius. Therefore the particle void is an influence factor that has to be taken into account when performing vortex research with PIV. An example of how particle voids appear is given in Fig. 2 at two positions (1), where the centers of two vortices can be identified due to their voids.

Experimental setup

The experiments took place in the rotor test facility (RTG) at the German Aerospace Center in Göttingen. The inflow to the vertically mounted 1.3 m diameter rotor is provided by an open circuit (Eiffel) wind tunnel with a square 1.6 m by 1.6 m nozzle. Due to the vertical alignment of the rotor an operation in ground effect is avoided. The rotor wake flow is convected away outside the building. The two rotor blades are made from carbon fiber reinforced plastic with a foam core structure. The modern DSA-9A airfoil with $9\,\%$ thickness and a chord length of $c = 72$ mm is used. With the blades span of 490 mm this leads to an aspect ratio of 6.8. For the tip design the parabolic ONERA SPP8 blade tip without anhedral was chosen. To account for the increasing Mach number towards the tip a negative linear twist of $-9.3°$ around the quarter chord line along the span is incorporated. The manually adjusted pitch links allow for a pitch angle setting with an accuracy of $\pm 0.1°$. A detailed description of the design and construction process of the RTG is given by Schwermer et al. 2016.

The experiments presented in this paper were part of the dynamic stall measurement campaign presented by Schwermer et al. 2017, and the same rotor operation parameters were used as shown in Tab. 1. However, this paper focusses on the evaluation of the blade tip vortices during a dynamic stall test case. The rotor was operated with a rotational frequency of 23.6 Hz which leads to a Mach number of 0.21 and a chord based Reynolds number of $350{,}000$, both at 75% rotor radius. In order to ensure the convection of the rotor wake and to provide a defined inflow the wind tunnel speed was set to a constant inflow of 2.2 m/s. To monitor the blade root pitch angles measured with Hall sensors a Datatel 30 channel telemetry system was mounted to the rotor head. This system with a bandwidth of 19 kHz and a resolution of 14 bit per channel also recorded signals from various other sensors like unsteady Kulite blade pressure transducers, strain gages and temperature sensors. A stationary Dewetron measurement system operating at 50 kHz was used to record inflow parameters, rotor head forces and moments as well as timing signals of the PIV system. The synchronization of the different measurement system was achieved by distributing an IRIG-B time code signal to each of them.

Table 1: Measurement parameters

Parameter	Values
Ω	$23.6\ 1/\text{s}$
M_{75}	0.21
$\text{Re}_{(c,75)}$	$350{,}000$
k_{75}	0.07
Θ_{75}	$16.9° + 6.2° \sin(2\pi\Omega t)$
V_∞	$2.2\ \text{m/s}$

The stereoscopic PIV system was aligned with the measurement plane located in the blades' wake, oriented in span-wise direction as depicted in Fig. 2. To guarantee high accuracy measurements the PIV system was set up following the advices given by Raffel et al. 2007.

Karlsruhe, Germany, ISBN 978-3-9816764-3-3

Several radial planes at azimuthal angles $\Psi_V = 7°, 10°, 20°, 30°$ and $40°$ behind the blade (vortex age) were investigated by adjusting the delay time between the blade passage and the laser trigger. The vortex ages are defined with respect to the $c/4$-line. To capture the entire pitching cycle of the blade, the outer usually stationary part of the swashplate was rotated by a stepper motor as described by Schwermer et al. 2017. This enables to sweep through the pitch cycle at the fixed azimuthal location of the PIV light sheet. Three Laskin nozzle generators with each 45 individual nozzles (PIVTEC, PIVpart45) were used to generate seeding particles. A rake installed in the wind tunnel settling chamber was used to homogeneously distribute these di-ethyl-hexyl sebacate (DEHS) droplets in rotor the inflow. The particle images were acquired with two pco.dimax cameras in double frame mode with a resolution of 2016 by 2016 pixels leading to a field of view with a size of 250 mm by 250 mm. A Continuum Surelite III dual cavity PIV laser with 380 mJ energy output per pulse at a wavelength of 532 nm was used to provide the illumination. Due to high out-of-plane velocities a time delay between the double pulses of 5 µs was chosen to minimize particle loss. The LaVision Davis 8.2.2 software was used for the evaluation of the raw particle image pairs. A combined multi-grid, multipass algorithm with a final interrogation window size of 24 by 24 pixels with 75 % overlap was chosen for image evaluation. No post processing was used after the last correlation pass. The resulting vector spacing is approximately 0.8 mm which corresponds to about 10 vectors within the vortex core. No evidence of peak locking was observed in histogram tests on random samples. The measurement uncertainty of the PIV setup is discussed in detail by Schwermer et al. 2017. Due to frequency limitations of the laser system all optical techniques were recorded at every third rotor revolution which equals 7.9 Hz. This means that every PIV image is acquired three revolutions after the previous image. With this system 2800 images were acquired during one swashplate rotation, corresponding to one pitch cycle.

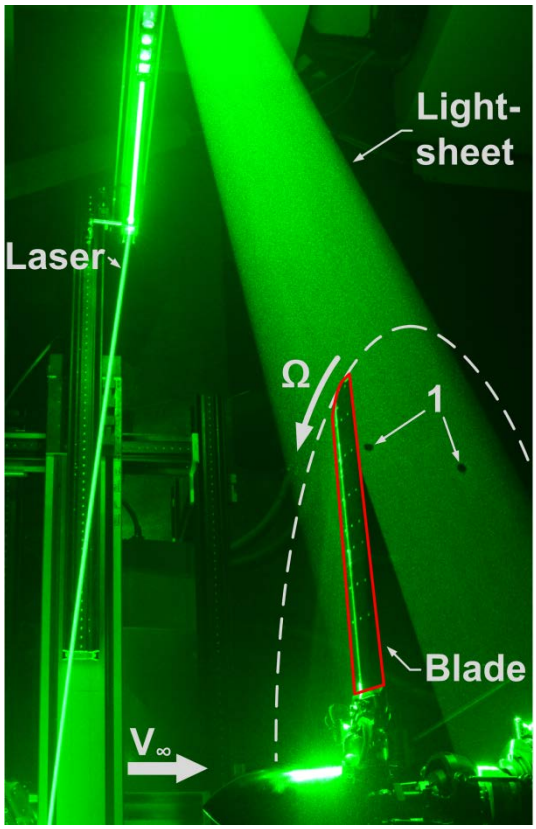

Figure 2: Experimental setup with illuminated laser light sheet and particle voids.

Data evaluation

The PIV evaluation leads to 2800 vector fields including the in-plane velocity components (v,w) and the out-of-plane velocity component u. These vector fields were further analyzed using Matlab in order to extract the positions and properties of the blade tip vortices. In the first velocity field of the PIV series, the approximate position of the vortex was selected by hand as an initial start value. This position is used to define a region of interest (ROI) which includes the vortex structure but excludes peripheral areas without relevant flow information but probable error sources (such as laser light reflections at the blade surface). The exact position of the vortex center in the ROI can now be identified using well-known vortex criteria. The current approach applies the “swirling strength”-criterion λ_{Ci} introduced by Zhou et al.

Karlsruhe, Germany, ISBN 978-3-9816764-3-3

1999, which is based on an Eigenvalue analysis of the in-plane velocity gradients $\nabla(v,w)$. Following the argumentation by Wolf et al. 2016, the vortex center is now defined as the centroid of λ_{Ci}. (A cut-off value of 50% of the maximum swirl in the ROI was introduced to remove residual noise.) This procedure is repeated for each vector field of the measurement series, and the ROI of successive vector fields is defined using the vortex position information of preceding fields. Fig. 3 shows the distribution of the out-of-plane velocity at a vortex age of $\Psi_{\mathrm{V}} = 30°$ for two different times within the pitching period. Fig. 3-left depicts the vortex of high-lift attached flow at a pitch angle of $\Theta_{75} = 21.6°$ on the upstroke, whereas Fig. 3-right displays data at the same pitch angle within stall conditions on the downstroke. In both images the detected vortex center is shown.

With respect to the previously defined vortex center the tangential velocity profile $V_{\mathrm{tang}}(\mathrm{r})$ of the vortices was calculated. With the assumption of rotationally symmetric vortices – which fits less well for vortices of separated flow condition than for those of attached flow – a radial binning with a step width of approximately 0.8 mm (according to the PIV resolution) was introduced. Within these bins the in-plane components of the velocity were used to calculate a mean tangential velocity.

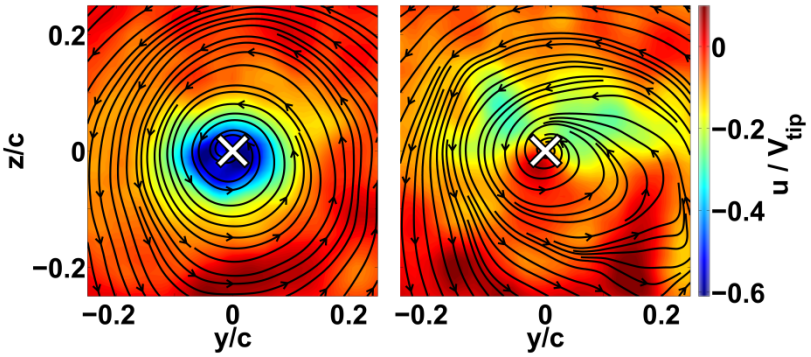

Figure 3: Out-of-plane velocity and in-plane streamlines at $\Psi_{\mathrm{V}} = 30°$ and $\Theta_{75} = 21.6°$; upstroke (left) and down-stroke (right); the crosses symbolize the detected vortex centers.

The maximum of the tangential velocity was estimated and its radial position was stored as the vortex core radius $\mathrm{r_c}$. The circulation then was calculated according to the previously defined equation $\Gamma = 2\,\pi\,r\,V_{\mathrm{tang}}(r)$.

Results

The results obtained from the measurement campaign are presented in Figs. 4 to 6. On the x-axis the pitching period t/T is displayed. $t/T = 0$ refers to the lowest angle of incidence. Phases up to $t/T = 0.5$ represent the upstroke of the blade reaching the maximum angle of incidence at $t/T = 0.5$. t/T higher than 0.5 represents the downstroke, respectively.

All data shown has been low pass filtered over the period with a sliding average filter of $dt/T = 0.0075$ (2.7° of azimuth). For better readability only every 20^{th} data point is plotted.

In Fig. 4 the circulation at $r = 0.2c$ ($\Gamma_{0.2\mathrm{c}}$) is depicted. For comparability reasons the values have been normalized by the product of the chord length c and the blade-tip velocity V_{tip}. Recent investigations Wolf et al. 2016 showed that the usage of $\Gamma_{0.2\mathrm{c}}$ is a suitable parameter taken as a substitute for the entire circulation Γ_0 when the observation window is limited.

The five graphs in Fig. 4 represent the five different vortex ages captured during the measurement. Apart from $t/T = 0.6$ to 0.8, $\Gamma_{0.2\mathrm{c}}$ describes a sinusoidal sweep between 0.14 in minimum (at $t/T = 0$ and 1) and 0.47 in maximum (at approximately $t/T = 0.5$). This behavior underlines the tight relationship between pitch angle, lift, and circulation during phases of attached flow. Within the region of $t/T = 0.6$ to 0.8 a circulation deficit occurs. This interval was identified to be subject to dynamic stall for the given measurement conditions by Schwermer et al. 2017. Therefore the decrease of circulation fits well to the decrease of lift

Karlsruhe, Germany, ISBN 978-3-9816764-3-3

as expected within stall. In particular, $\Gamma_{0.2c}$ is a parameter characterizing vortices in close agreement to the lift distribution.

A vertical cut through the graphs in Fig. 4 corresponds to the concept of following one specific vortex, which has been formed at a certain normalized time and therefore at a certain angle of incident, over its age Ψ_V. Within attached flow conditions young vortices have a slightly lower circulation than vortices of higher age. An explanation for this tendency is the roll up auf vorticity from the outer blade wake into the vortex which leads to a rising $\Gamma_{0.2c}$. In stall conditions however an inversed behavior is observed: The stall-related break-down of circulation is rather small for young vortices (about 30% compared to the respective attached-flow condition) than for older vortices (about 70%). During stalled phases, the tip vortex circulation decreases with increasing vortex age. An explanation can be found in the rather turbulent wake flow of the separated blade regions further inboards, leading to higher dissipation and thus a comparably high circulation deficit at high vortex ages compared to younger ones. In addition, other investigations show that stall is delayed at the blade tip due to the blade-tip vortex influence (see Schwermer et al. 2017). This phenomenon also fits the observation of less reduced circulation in young vortices that have not yet been influenced by the blade wake shedding from blade regions further inboard. At the time of reattachment the circulation deficit is regained rather quickly.

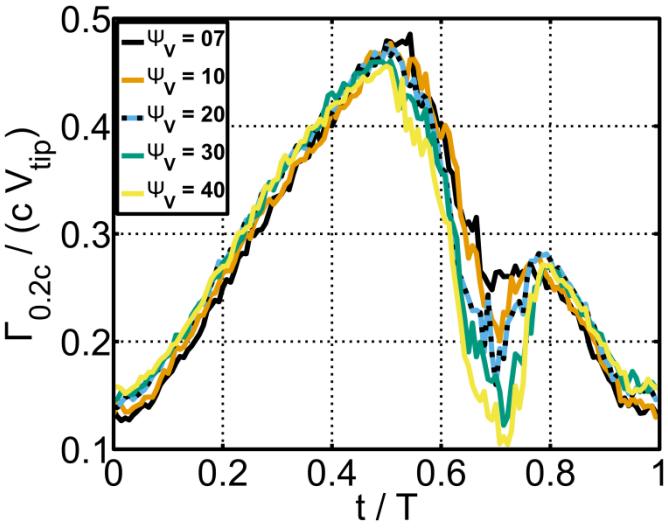

Figure 4: Development of circulation Γ at $r = 0.2c$ over the pitching period.

In Fig. 5 the maximal tangential velocity $V_{\text{tang, max}}$ over the pitching period is shown. The values have been normalized by the blade-tip velocity V_{tip}. The temporal development of $V_{\text{tang, max}}$ also follows a sinus-like curve within attached flow. In agreement to the formerly described loss in circulation also the maximum of the tangential velocity shows a deficit within stalled flow conditions.

When comparing the maximal tangential velocities of a vortex over its age, higher values of $V_{\text{tang, max}}$ can be observed for young vortices compared to old vortices formed at the same normalized time t/T. For low angles of incidence (at $t/T < 0.2$ and $t/T > 0.9$), the difference is small compared to higher angles of incidence and thus higher lift. Within stall conditions ($t/T = 0.6$ to 0.8) this general tendency is preserved as vortices of all measured ages exhibit the same velocity deficit.

The radial position of highest tangential velocity is defined as the vortex core

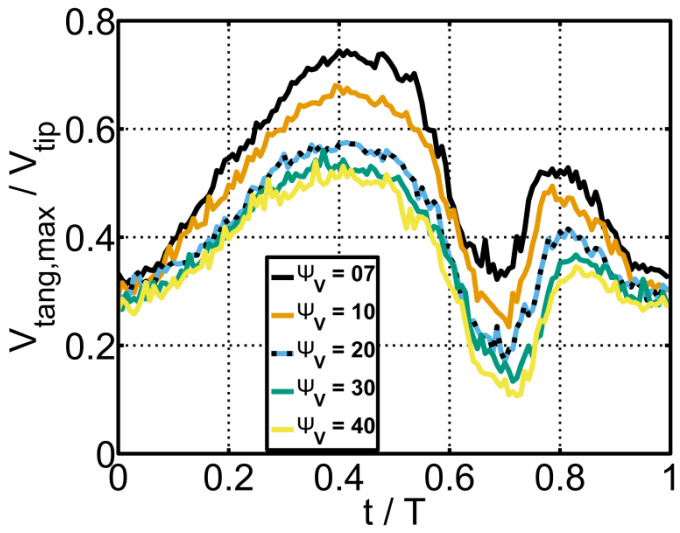

Figure 5: Development of the maximal tangential velocity $V_{\text{tang, max}}$ over the pitching period.

radius r_c. Extracting the maximal tangential velocity over time and its radial position with respect to the vortex center allows for a temporal description of the vortex core size. In Fig. 6 this development of the vortex core radius is depicted as percentage of chord length. Vortices at low angles of incidence show the smallest core radii. With an increasing pitch angle and an increasing lift also the core radii grow. Within a normalized time of $t/T = 0.2$ to 0.5 for high vortex ages a rather large particle void compared to the vortex core radius is observed. Therefore the core radii of old vortices within this time interval have to be considered to be slightly larger than the values given in Fig. 6. Particularly the core radii for the ages $\Psi_V = 30°$ and $40°$ are less reliable, which can be seen from the comparably high fluctuations over the normalized time.

The highest radii for all vortex ages are reached at approximately $t/T = 0.65$. At this point there is the maximum extent of the recirculation area over the suction side of the blade according to research by Schwermer et al. 2017. Within stall conditions ($t/T = 0.6$ to 0.8) the core radii vary strongly and a reliable detection of the core radius is difficult due to the high fluctuations in combination with the rather low values of $V_{\text{tang, max}}$ highlighted in Fig. 5. Reattachment goes along with a rapid decrease of the vortex core radii of all vortex ages (see Fig. 6).

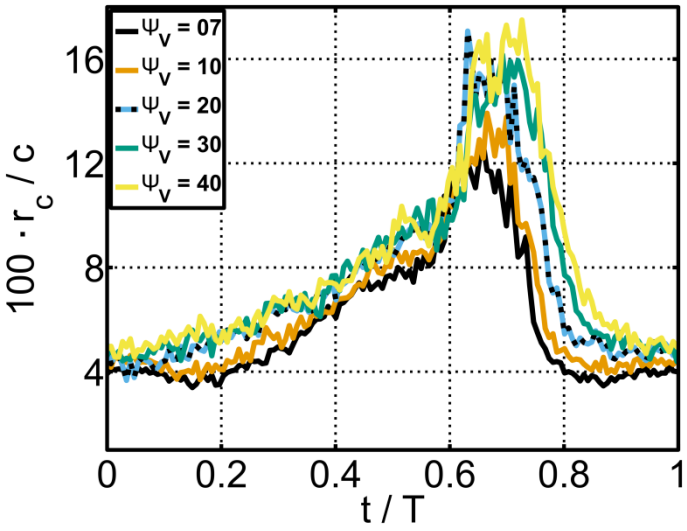

Figure 6: Development of the vortex core radius r_c over the pitching period.

Comparing the vortex radii as a function of vortex age, a slightly growing tendency can be observed over almost the whole period. The largest changes over the vortex age occur during reattachment. In general, vortices of all ages show a rapid decrease in size, but the time instant of the reattachment depends on the vortex age: At a normalized time of $t/T = 0.8$ a young vortex shows an already shrunk vortex core radius and can thus be related to reattached flow conditions. At the same normalized time older vortices in contrast show larger core radii that go along with separated flow. This implies that around reattachment the vortex is affected differently depending on its age. A possible explanation might be that the already reattached blade-tip region forms an initially compact vortex, but then turbulence shed from still separated regions of the blade being rolled up into the vortex influences the vortex within its development. This phenomenon also goes along with the change in circulation and maximal tangential velocity as discussed before.

Conclusion and Outlook

Within this work stereoscopic PIV measurements have been performed at the rotor test facility RTG in Göttingen. Measuring all three velocity components allowed for a comprehensive analysis of vortices generated at a rotor in dynamic stall conditions. Five radial planes at vortex ages of $\Psi_V = 7°, 10°, 20°, 30°, 40°$ have been investigated and the core radii, the tangential velocities and also the circulation of the vortices have been computed. The discussion of the results showed strong influences of the pitching motion on the vortex generation but also on the temporal development. These findings support the idea that the topology of the blade wake interacts with the developing vortex, changing its characteristics. The temporal change

of vortex properties implies a change along the vortex tube. Further research therefore should focus on the axial vortex properties and the exact interaction of blade vortices and the blades wake. Furthermore techniques to reduce the particle void have to be considered.

References

Bauknecht, A., Ewers, B., Schneider, O., Raffel, M., 2017: "Blade tip vortex measurements on actively twisted rotor blades", Experiments in Fluids, Vol. 58, No. 49.

Poling, D. R., Dadone, L., Telionis, D. P., 1989: "Blade-Vortex Interaction", AIAA Journal, Volume 27, No. 6, pp. 694-699.

Raffel, M., Willert, C. E., Wereley, S. T., Kompenhans, J., 2007: "Particle Image Velocimetry – A Practical Guide", 2nd ed., Springer, Berlin.

Schwermer, T., Richter, K., Raffel, M., 2016: "Development of a Rotor Test Facility for the Investigation of Dynamic Stall", New Results in Numerical and Experimental Fluid Mechanics X, Notes on Numerical Fluid Mechanics and Multidisciplinary Design, Volume 132, pp 663-673.

Schwermer, T., Gardner, A. D., Raffel, M., 2017: "Dynamic Stall Experiments on a Rotor with High Cyclic Setting in Axial Inflow", American Helicopter Society 73rd Annual Forum, Fort Worth.

Tangler, J. L., 1977: "Schlieren and Noise Studies of Rotors in Forward Flight", American Helicopter Society 33rd Annual National Forum.

Wolf, C. C., Merz, C. B., Richter, K., Raffel, M., 2016: "Tip-Vortex Dynamics of a Pitching Rotor Blade Tip Model", AIAA Journal, Volume 54, No. 10, pp. 2947-2960.

Young, L. A., 2003: "Vortex Core Size in the Rotor Near-Wake", NASA Technical Memorandum 2003-212275.

Zhou, J., Adrian, R. J., Balachandar, S., Kendall, T. M., 1999: "Mechanism for Generating Coherent Packets of Hairpin Vortices in Channel Flow", Journal of Fluid Mechanics, Volume 387, pp. 353-396.

Karlsruhe, Germany, ISBN 978-3-9816764-3-3